



**HAL**  
open science

## A Comparative Investigation of the Role of the Anchoring Group on Perylene Monoimide Dyes in NiO-Based Dye-Sensitized SolarCells

Ilaria Ciofini, Yoann Farré, Federica Maschietto, Jens Fohlinger, Mike Wykes, Aurélien Planchat, Pellegrin Yann, Errol Blart, Leif Hammarstrom, Fabrice Odobel

► **To cite this version:**

Ilaria Ciofini, Yoann Farré, Federica Maschietto, Jens Fohlinger, Mike Wykes, et al.. A Comparative Investigation of the Role of the Anchoring Group on Perylene Monoimide Dyes in NiO-Based Dye-Sensitized SolarCells. ChemSusChem, 2020, 10.1002/cssc.201903182 . hal-02879287

**HAL Id: hal-02879287**

**<https://hal.science/hal-02879287>**

Submitted on 13 Nov 2020

**HAL** is a multi-disciplinary open access archive for the deposit and dissemination of scientific research documents, whether they are published or not. The documents may come from teaching and research institutions in France or abroad, or from public or private research centers.

L'archive ouverte pluridisciplinaire **HAL**, est destinée au dépôt et à la diffusion de documents scientifiques de niveau recherche, publiés ou non, émanant des établissements d'enseignement et de recherche français ou étrangers, des laboratoires publics ou privés.

# A comparative investigation of the role of anchoring group on perylene monoimide dyes in NiO based dye-sensitized solar cells

Yoann Farré,<sup>a</sup> Federica Maschietto,<sup>b</sup> Jens Föhlinger,<sup>c</sup> Mike Wykes,<sup>b</sup> Aurélien Planchat,<sup>a</sup> Yann Pellegrin,<sup>a</sup> Errol Blart,<sup>a</sup> Iliaria Ciofini,<sup>\*b</sup> Leif Hammarström,<sup>\*c</sup> Fabrice Odobel<sup>\*a</sup>

<sup>a</sup>*Université LUNAM, Université de Nantes, CNRS, Chimie et Interdisciplinarité: Synthèse, Analyse, Modélisation (CEISAM), UMR 6230, 2 rue de la Houssinière, 44322 Nantes cedex 3, France. E-mail: [Fabrice.Odobel@univ-nantes.fr](mailto:Fabrice.Odobel@univ-nantes.fr)*

<sup>b</sup>*PSL Research University, Institut de Recherche de Chimie Paris IRCP, CNRS-Chimie ParisTech, 11 rue P. et M. Curie, F-75005 Paris 05, France. E-mail: [ilaria.ciofini@chimie-paristech.fr](mailto:ilaria.ciofini@chimie-paristech.fr)*

<sup>c</sup>*Uppsala Universitet, Department of Chemistry – Ångström Laboratories, Box 523, 751 20 Uppsala, Sweden E-mail: [leif.hammarstrom@kemi.uu.se](mailto:leif.hammarstrom@kemi.uu.se)*

## Abstract

The anchoring group of a sensitizer may strongly affect the overall properties and stability of the resulting dye sensitized solar cells (DSSCs) and dye sensitized photoelectrosynthetic solar cells (DSPECs). This article describes a comprehensive study of the properties of seven perylene monoimide dyes (PMI) for their immobilization on nanocrystalline NiO film. The PMI dyes differ only by the nature of the anchoring group, which are: carboxylic acid (**PMI-CO<sub>2</sub>H**), phosphonic acid (**PMI-PO<sub>3</sub>H<sub>2</sub>**), acetyl acetone (**PMI-acac**), pyridine (**PMI-Py**), aniline (**PMI-NH<sub>2</sub>**), hydroxyquinoline (**PMI-HQ**), and dipicolic acid (**PMI-DPA**). The dyes were investigated by cyclic voltammetry, spectroelectrochemistry, modeled by DT-DFT quantum chemical calculations. The mode of binding of these anchoring groups was

investigated by infrared spectroscopy and the stability of the binding to NiO surface was studied by desorption experiments in acidic and basic media. Overall, we found that phosphonic acid group offers the strongest binding to NiO surface in terms of stability and dye loading. Finally, a photophysical study by ultrafast transient absorption spectroscopy shows that all dyes inject a hole in NiO with rate constants on a subpicosecond timescale and display similar charge recombination kinetics. The photovoltaic properties of the dyes show that **PMI-HQ** and **PMI-acac** gave the highest photovoltaic performances due to lower degree of aggregation on the surface.

## Introduction

NiO based dye-sensitized photocathodes have enjoyed a rising popularity in the scientific community because they are the key component of tandem dye sensitized solar cells (DSSCs)<sup>[1-3]</sup> and dye sensitized photoelectrosynthetic solar cells (DSPECs).<sup>[4-6] [7-8]</sup> These devices rely on chemically bound molecular components (sensitizers, or sensitizer + catalysts) to a NiO mesoporous electrode.<sup>[9]</sup> In DSPECs, the catalyst can be either covalently connected to the dye or co-adsorbed on the NiO surface. The primary role of the sensitizer is to absorb light and inject a hole in the valence band of NiO with the highest quantum yield upon photoexcitation.<sup>[10-11]</sup> This requirement demands a significant electronic coupling between the dye excited state and the valence band manifold. On the other hand, the catalyst must accumulate reductive equivalents and catalyze the reduction of substrates in solution before charge recombination takes place. This function requires slow charge recombination rate constant and consequently a weak electronic interaction between the injected holes in NiO and the reduced catalyst. Accordingly, the dye and the catalyst require different connectors if they are to be co-adsorbed on the surface. However, both dyes and catalysts must remain strongly attached to the NiO surface to sustain long operation lifespan. This condition is quite satisfyingly met in DSSCs, while it still remains an important challenge to solve in DSPECs, because the latter usually operate in harsher conditions than DSSC, most often in aqueous acidic or basic media. Thus, the anchoring group represents a very important factor to consider for the optimal design of sensitizers and dye/catalyst for NiO based DSSCs or DSPECs, because it controls both the electronic coupling and the stability of the anchored molecules on the NiO surface. The impact of different anchoring groups in TiO<sub>2</sub> based photoanodes has been quite thoroughly investigated,<sup>[12-13]</sup> although many of these studies are

rather recent if one considers the large amount of work undertaken on Grätzel cells since 1991.<sup>[14-15]</sup> The development of NiO based photocathodes has been much less explored than the TiO<sub>2</sub> based photoanodes, therefore it is unsurprising that there are few studies of the role of the anchoring group on NiO dyes, for which carboxylic acid remains the most used one.<sup>[9]</sup> However, the electronic properties of the optimal binding group for NiO are certainly different as those for TiO<sub>2</sub> based photoanodes, because NiO is a p-type semiconductor and is composed of Ni(II) cation which is a weaker Lewis acid than Ti(IV) in TiO<sub>2</sub>. For a fast hole injection into the NiO valence band, the HOMO of the dye must mix with the valence band, which implies that the anchoring group orbitals must give a significant contribution to the HOMO. This is the opposite situation for TiO<sub>2</sub> sensitizers, which must be composed of electron deficient anchoring groups on which the LUMO should be delocalized.<sup>[16]</sup> We have investigated the replacement of carboxylic acid by catechol,<sup>[17]</sup> carbodithioic acid,<sup>[17]</sup> phosphonic acid,<sup>[17]</sup> acetyl acetone (acac),<sup>[18]</sup> silyl<sup>[19]</sup> and other teams have investigated pyridine,<sup>[20-22]</sup> di(carboxylic acid)pyrrole,<sup>[23-24]</sup> hydroxamic acid,<sup>[25]</sup> and di(carboxylic acid)triazole<sup>[26]</sup> as alternative anchoring groups for NiO photocathodes. Owing to the scarcity of systematic studies on NiO anchoring groups, we have been interested to investigate the properties of a series of dyes that differ only by the nature of the anchoring group (Chart).

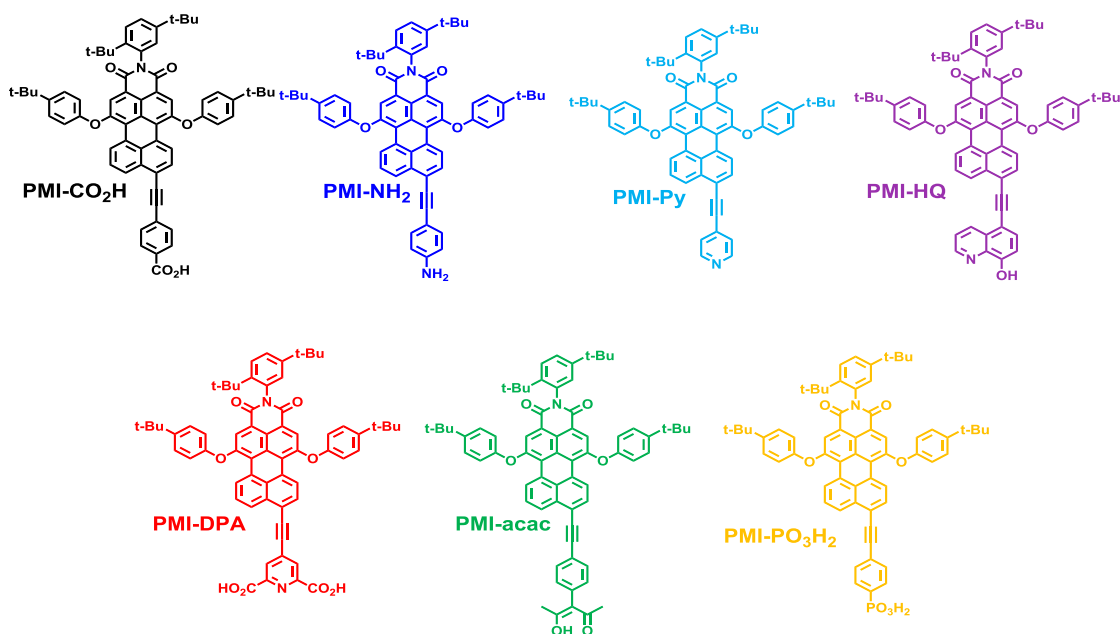


**Chart.** Structures of the PMI dyes investigated in this study.

As dye for this study, perylene monoimide (PMI) was chosen as an ideal candidate for this study because previous work has shown that it is an effective NiO sensitizer and the radical anion displays a characteristic absorption band, which makes it easy to detect by transient absorption spectroscopy.<sup>[27-28]</sup> In this work, we prepared and investigated PMI dyes connected to seven different anchoring groups *via* an ethynyl spacer in order to promote electronic interaction of the  $\pi$ -aromatic system of PMI with the anchoring group (Chart). The PMI dye was substituted with pyridine (**PMI-Py**), aniline (**PMI-NH<sub>2</sub>**), phosphonic acid (**PMI-PO<sub>3</sub>H<sub>2</sub>**), hydroxyquinoline (**PMI-HQ**), acetyl acetone (**PMI-acac**), dipicolic acid (**PMI-DPA**), and naturally the carboxylic acid derivative (**PMI-CO<sub>2</sub>H**) was synthesized for purpose of comparison. The experimental electronic absorption, emission and electrochemical properties of the dyes were measured and analyzed by quantum chemical calculations. The dyes were also grafted on NiO mesoporous films and the stability of the linkage was assessed by desorption studies. The hole injection efficiency was determined by photovoltaic measurements in p-DSSCs and by ultrafast transient absorption spectroscopy.

## Results and discussion

The synthesis and characterization of the dyes, preparation and sensitization of the NiO films and experimental methods are described in the Supporting Information.

### Electronic UV-visible absorption and emission spectroscopy

First, the absorption and emission spectra of the all dyes were recorded in DMF solution at room temperature (Figures 1 and 2). The spectroscopic data including wavelengths of maximum absorption wavelength ( $\lambda_{\text{abs}}$ ), extinction coefficient ( $\epsilon$ ), maximal emission wavelength ( $\lambda_{\text{em}}$ ) and the zero-zero energy level of the lowest singlet excited state ( $E_{00}$ ) are collected in Table 1.

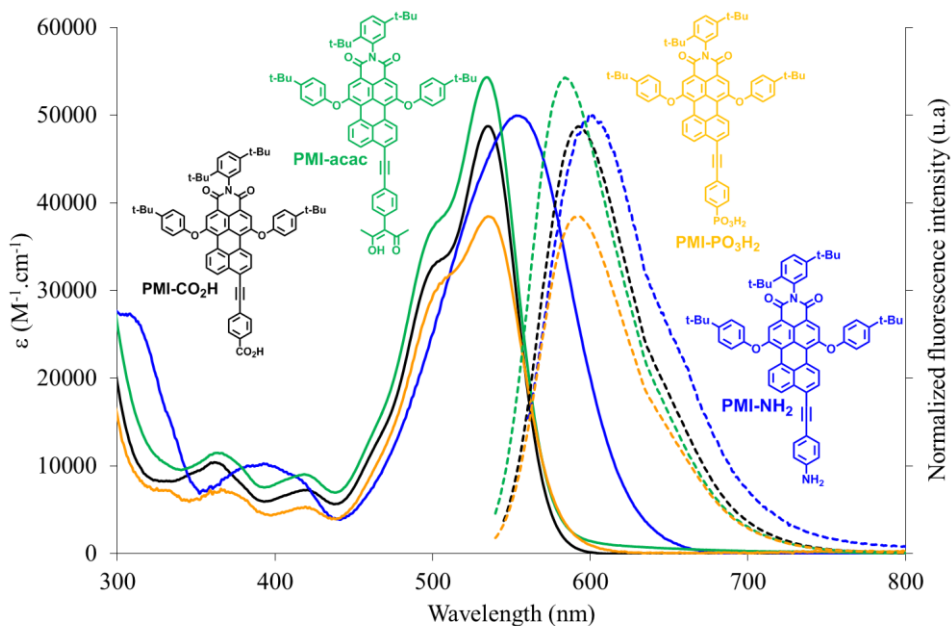


**Figure 1.** Electronic absorption (straight line) and normalized steady state emission (dashed line) spectra of the **PMI-CO<sub>2</sub>H**, **PMI-acac**, **PMI-PO<sub>3</sub>H<sub>2</sub>** and **PMI-NH<sub>2</sub>** dyes recorded in DMF solution.

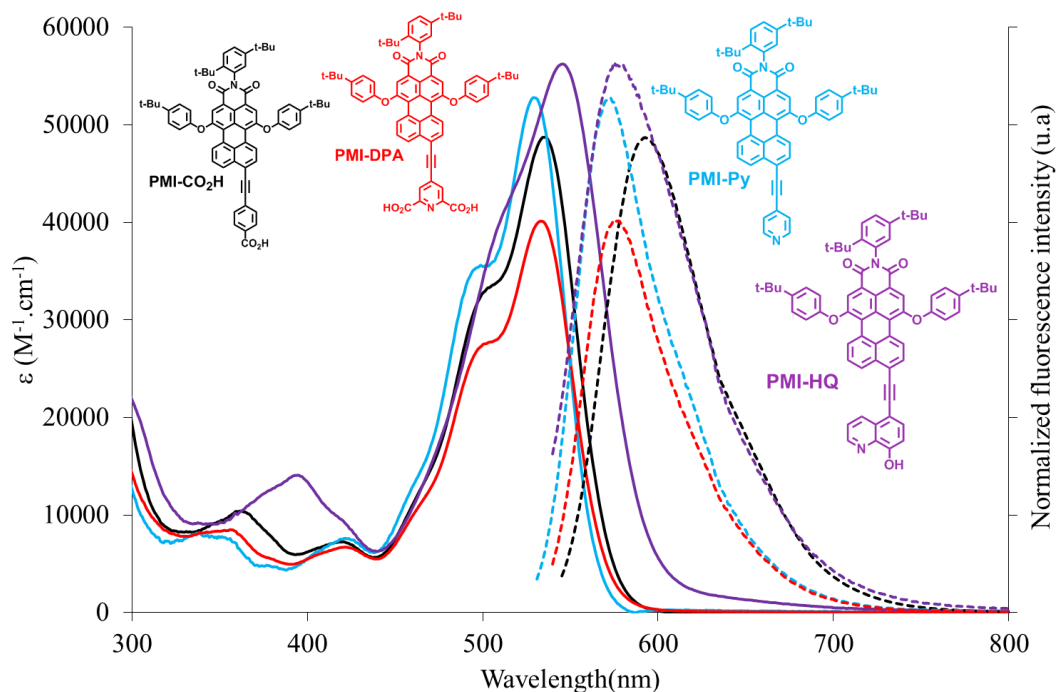


**Figure 2.** Electronic absorption (straight line) and normalized steady state emission (dashed line) spectra of the **PMI-CO<sub>2</sub>H**, **PMI-DPA**, **PMI-Py** and **PMI-HQ** dyes recorded in DMF solution.

The absorption spectra of **PMI-CO<sub>2</sub>H**, **PMI-acac**, **PMI-PO<sub>3</sub>H<sub>2</sub>**, **PMI-DPA** and **PMI-Py** exhibit a structured and intense absorption band around 480-580 nm, attributed to a  $\pi$ - $\pi^*$  transition localized on the PMI moiety with similar  $\epsilon$  values around  $45000 \text{ M}^{-1}\text{cm}^{-1}$  at the maximum wavelength, in agreement with similar dyes. **PMI-NH<sub>2</sub>** and **PMI-HQ** exhibit a red-shifted absorption band compared to the above dyes. This is attributed to the electron donating effect of the aniline and phenol groups that destabilize the HOMO level and consequently lower the optical gap and also leads to a charge transfer character of the optical absorption in which the PMI acts as an electron accepting unit (Figures 1 and 2). This is also supported by DFT calculations (see below). Consequently, these two dyes display a broader absorption spectral coverage than the others. Moreover, all these PMI dyes exhibit a strong fluorescence band with a maximum emission located at 560-600 nm. From the absorption and emission spectra, we derive a singlet excited state energy ( $E_{00}$ ) of about 2.2 eV (Figures 1&2 and Table 1).

**Table 1.** Wavelengths of maximal absorption ( $\lambda_{\text{abs}}$ ) with extinction coefficient ( $\epsilon$ ), wavelength of maximal emission ( $\lambda_{\text{em}}$ ) recorded at room temperature and zero-zero energy level of the lowest singlet excited state ( $E_{00}$ ) of the PMI moiety.

Dyes	<sup>a</sup> $\lambda_{\text{abs}}/\text{nm}$ ( $\epsilon/\text{M}^{-1}\text{cm}^{-1}$ )	<sup>b</sup> $\lambda_{\text{abs}}/\text{nm}$	$\lambda_{\text{em}}/\text{nm}$	<sup>c</sup> $E_{00}/\text{eV}$
<b>PMI-CO<sub>2</sub>H</b>	535 (48800) ; 421 (7300) ; 362 (10400)	495	592	2.21
<b>PMI-NH<sub>2</sub></b>	555 (49900) ; 393 (10300)	-	601	2.14
<b>PMI-Py</b>	529 (52800) ; 422 (7600) ; 338 (8200)	-	573	2.25
<b>PMI-DPA</b>	534 (40100) ; 422 (6700) ; 357 (8500)	497	575	2.24
<b>PMI-HQ</b>	546 (56200) ; 395 (14100)	514	575	2.21
<b>PMI-Acac</b>	534 (54300) ; 419 (9100) ; 363 (11500)	497	584	2.22
<b>PMI-PO<sub>3</sub>H<sub>2</sub></b>	535 (38500) ; 419 (5300) ; 366 (7400)	495	563	2.20

<sup>a</sup>recorded in dichloromethane solution. <sup>b</sup>recorded on thin NiO film. <sup>c</sup>calculated according to the equation:  $E_{00} = 1240/\lambda_{\text{inter}}$ , where  $\lambda_{\text{inter}}$  is the wavelength at the intersection of the normalized absorption and emission spectra in dichloromethane.

The absorption spectra of these PMI dyes were then investigated after chemisorption on thin NiO films (Figure 3). All dyes, except **PMI-Py** and **PMI-NH<sub>2</sub>**, turn the initially greyish NiO film into a reddish film after soaking the electrode into a DMF solution of these dyes. Contrary to our expectation, the aniline and pyridyl groups do not show strong affinity to NiO surface, in spite of the fact that some previous reports showed that they could bind to some metal oxides, including NiO for pyridine.<sup>[20-22]</sup> The electron withdrawing effect of PMI might decrease the electron density on these amines and consequently diminish their ability to coordinate to nickel.

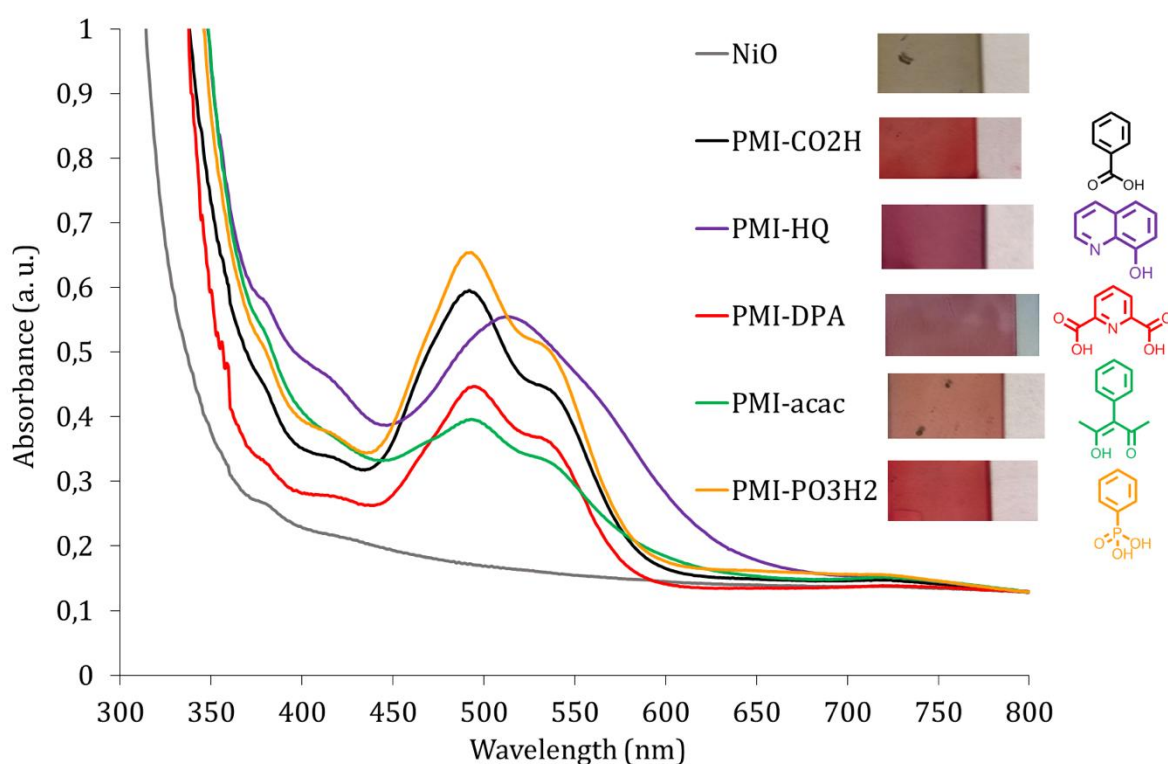


**Figure 3.** Electronic absorption spectra of the **PMI-CO<sub>2</sub>H**, **PMI-HQ**, **PMI-DPA**, **PMI-acac** and **-PMI-PO<sub>3</sub>H<sub>2</sub>** dyes recorded in thin films of NiO and pictures of the corresponding NiO thin films.



Interestingly, the visible absorption band is blue-shifted and the intensity ratio of the vibronic peaks (between 450 and 550 nm) is inverted with respect to those in solution (Figures 1-2 and S2 and Table 1). These characteristics are clear indications of the formation of H-type aggregates on NiO surface and is due to excitonic interaction between stacked chromophores.<sup>[29-31]</sup>

Finally, the dye loading of these PMI dyes on NiO was determined by desorption experiments. Towards this end, we have not used the classical strategy consisting of soaking the NiO electrodes into a basic solution of hydroxyde, because PMI dyes are not fully stable under such conditions. Instead, the PMIs were cleanly and quickly desorbed from the NiO surface by a DMF solution of phenyl phosphonic acid which acts as a competing ligand.<sup>[32]</sup> The average values of dye loadings were determined from three independent runs and they are indicated in Figure 4.

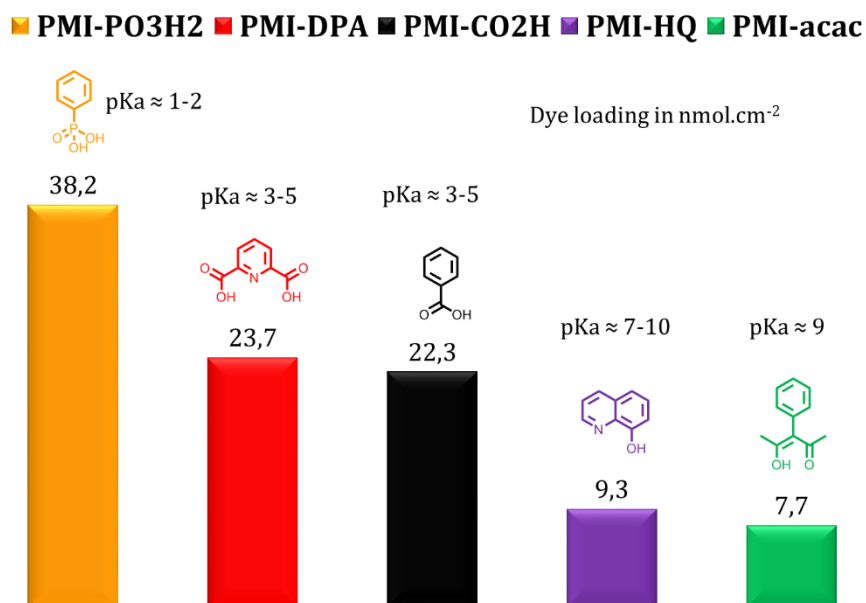


**Figure 4.** Dye loading values (in nmol/cm<sup>2</sup>) of the PMI dyes measured on NiO film of 1.3 μm thickness. The average pKa value is given above each anchoring group.

Phosphonic acid is undoubtedly the strongest binding group, then comes dipicolinic acid closely followed by carboxylic acid and finally hydroxyquinoline and acac, which gave the lowest loading on NiO. The dye loading and the stability of the linkage on NiO (see below)

are strongly related to the pKa of the anchor group, with the usual observation that strongly acidic binding groups displays higher affinity to the metal oxide surface.<sup>[12-13]</sup>

### Electrochemistry, spectroelectrochemistry and calculations of the charge transfer driving forces

These dyes were studied by cyclic voltammetry to determine the potentials for their first reduction and oxidation, as well as to calculate the hole injection ( $\Delta G^\circ_{inj}$ ) and dye regeneration ( $\Delta G^\circ_{reg}$ ) driving forces with iodine and tetrazole-thiol ( $T_2/T^-$ ) based electrolytes (Table 2 and Figure S1 for the structures of  $T_2/T^-$ ).

All the PMI dyes show similar behavior in cyclic voltammetry. For each dye, one reversible reduction process occurs at -0.9 V vs. SCE corresponding to the addition of an electron on the PMI unit. Conversely, in the anodic region, the PMI core is oxidized at around 1.1 - 1.2 V vs. SCE with a non-reversible wave for the dyes **PMI-CO<sub>2</sub>H**, **PMI-acac**, **PMI-Py**, **PMI-DPA** and **PMI-PO<sub>3</sub>H<sub>2</sub>**. For the dyes **PMI-NH<sub>2</sub>** and **PMI-HQ** the first oxidation is cathodically shifted by circa 300 mV relative to the others PMI dyes reflecting the electron donating effect of the electron rich anchoring group (destabilization of the HOMO level) consistent with the spectroscopic properties.

The Gibbs free energies of hole injection into the NiO valence band after excitation of the dye and that of the regeneration reaction with iodine or tetrazole thiol based electrolytes indicate that all PMI dyes display sufficient exergonicity, by a large margin, for the charge transfer processes to spontaneously occur (Table 2).

**Table 2.** Redox potentials recorded by cyclic voltammetry at room temperature in dichloromethane/DMF [95:5] solution with Bu<sub>4</sub>NPF<sub>6</sub> (0.1 M) as supporting electrolyte and referenced *versus* saturated calomel electrode (SCE). Calculated Gibbs free energies for hole injection ( $\Delta G^\circ_{inj}$ ) and dye regeneration ( $\Delta G^\circ_{reg}$ )

Dyes	$E_{a,peak}$ (PMI <sup>+</sup> /PMI) (V)	$E_{1/2}$ (PMI/PMI <sup>-</sup> ) (V)	$^aE$ (PMI*/PMI <sup>-</sup> ) (V)	$^b\Delta G^\circ_{inj}$ (eV)	$^c\Delta G^\circ_{reg}$ with I <sub>3</sub> <sup>-</sup> (eV)	$^d\Delta G^\circ_{reg}$ with T <sub>2</sub> /T <sup>-</sup> (eV)
<b>PMI-CO<sub>2</sub>H</b>	1.20	-0.93	1.28	-0.98	-0.61	-1.18

<b>PMI-NH<sub>2</sub></b>	0.83	-0.93	1.21	-0.91	-0.61	-1.18
<b>PMI-Py</b>	1.18	-0.91	1.34	-1.04	-0.59	-1.16
<b>PMI-DPA</b>	1.25	-0.90	1.34	-1.04	-0.58	-1.15
<b>PMI-HQ</b>	0.96	-0.94	1.27	-0.97	-0.62	-1.19
<b>PMI-acac</b>	1.10	-0.94	1.28	-0.98	-0.62	-1.19
<b>PMI-PO<sub>3</sub>H<sub>2</sub></b>	1.19	-0.97	1.23	-0.93	-0.65	-1.22

<sup>a</sup>Calculated according to the equation:  $E_{1/2}(\text{PMI}^*/\text{PMI}) = E_{1/2}(\text{PMI}/\text{PMI}) + E_{00}$ . <sup>b</sup>Calculated according to the equation:  $\Delta G_{\text{inj}}^{\circ} = E_{\text{VB}}(\text{NiO}) - E_{\text{Red}}(\text{PMI}^*/\text{PMI})$  with  $E_{\text{VB}}(\text{NiO}) = 0.30 \text{ V vs. SCE}$ .<sup>[33]</sup> <sup>c</sup>Calculated according to the equation:  $\Delta G_{\text{reg}} = E_{\text{Red}}(\text{PMI}/\text{PMI}) - E(\text{I}_3^-/\text{I}_2^{\bullet-})$  with  $E(\text{I}_3^-/\text{I}_2^{\bullet-}) = -0.32 \text{ V vs. SCE}$ .<sup>[34]</sup> <sup>d</sup>Calculated according to the equation:  $\Delta G_{\text{reg}} = E_{\text{Red}}(\text{PMI}/\text{PMI}) - E(\text{T}_2/\text{T}^{\bullet-})$  with  $E(\text{T}_2/\text{T}^{\bullet-}) = 0.25 \text{ V vs. SCE}$ .<sup>[35]</sup>

The spectra of the radical anions of **PMI-CO<sub>2</sub>H** and **PMI-HQ** were recorded by spectroelectrochemistry in dichloromethane with Bu<sub>4</sub>NPF<sub>6</sub> as supporting electrolyte to facilitate the interpretation of the photophysical study by transient absorption spectrometry (see below). The ground state absorption spectra of the **PMI-DPA**, **PMI-acac** and **PMI-PO<sub>3</sub>H<sub>2</sub>** being very close to that of **PMI-CO<sub>2</sub>H**, it is reasonable to conclude that the spectrum also of the radical anion would be very similar (Figures 1-2). The reduction of **PMI-CO<sub>2</sub>H** induces an important spectral change, which is accompanied by a bleach of the ground state absorption between 450-600 nm and the formation of a new band between 600-750 nm, which peaks at 654 nm. These changes are in perfect agreement with those measured with similar PMI dyes reported in the literature.<sup>[27-28]</sup> The same experiment run with **PMI-HQ** yields similar spectral changes except that the spectrum of the radical anion is broader and is stronger in the lower energy part of the visible spectrum ( $\lambda_{\text{max}} = 656 \text{ nm}$ ; Figure 5) as was also the case for the spectrum of the neutral dye above.

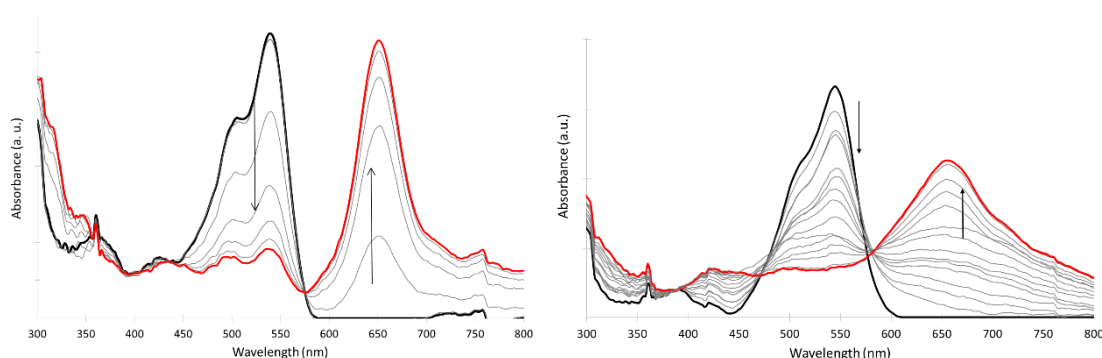


**Figure 5.** Evolution of the spectrum of the neutral for **PMI-CO<sub>2</sub>H** (left) and **PMI-HQ** (right) upon electrochemical reduction in dichloromethane. The initial spectrum of the neutral ground state is shown in black and the spectrum of the fully reduced dye is in red.

### **Binding mode of the anchoring group on NiO studied by infrared spectroscopy**

Characterization of the dye binding modes on the NiO surface was made by FTIR spectroscopy, as there is extensive information available on the position of vibrational transitions of these anchoring groups on TiO<sub>2</sub><sup>[12-13]</sup> but fewer on NiO.<sup>[18, 20, 36-37]</sup> To interpret the data, we have compared the FTIR spectra of the bare NiO with those of the dye in KBr pressed disc and the dye grafted on NiO in order to determine the band shifts and disappearances (Figures S1-S5). Figure 6 summarizes the binding mode of each dye deduced from the analysis of the FTIR spectra. First, the spectrum of bare NiO displays two broad bands: a weak one at 1631 cm<sup>-1</sup> attributed to the bending vibration mode of hydroxyl groups on the NiO surface<sup>[38]</sup> and the more intense one at 1346 cm<sup>-1</sup> assigned to the presence of adsorbed carbonate probably due to residual contaminants on the surface or coming from carbonization of the NiO paste used for screen printing.<sup>[39]</sup> Second, the intense C=O stretching band of the bisimide group, located at 1709 cm<sup>-1</sup> is observed on the IR spectra of all the PMI dyes without any modification before and after grafting on NiO. Naturally, this moiety is not involved in the binding with NiO, but bear witness of the presence of dye attached to the NiO surface.

Starting with **PMI-CO<sub>2</sub>H**, after binding to NiO, the carboxylic C=O stretching band seen in KBr as a shoulder at 1727 cm<sup>-1</sup> disappears upon binding on NiO. A new band appears at 1380 cm<sup>-1</sup>, which is attributed to the symmetric stretching of O-C-O (Figure S3). The difference in wavenumber between the asymmetric and symmetric stretching of O-C-O is generally used as a diagnostic tool to determine the binding mode of CO<sub>2</sub>H.<sup>[40-41]</sup> Unfortunately, the asymmetric stretch of O-C-O, which is known to show up between 1610 cm<sup>-1</sup> and 1650 cm<sup>-1</sup>,<sup>[40, 42-43]</sup> cannot be distinguished here because this region overlaps with the NiO vibration modes of hydroxyl groups. Although, we can confidently conclude that the PMI dye is coordinatively bound *via* its carboxylic acid group and exclude the monodentate ester like binding, it is impossible to safely determine if it is a bidentate chelating or bidentate bridging mode (Figure 6).

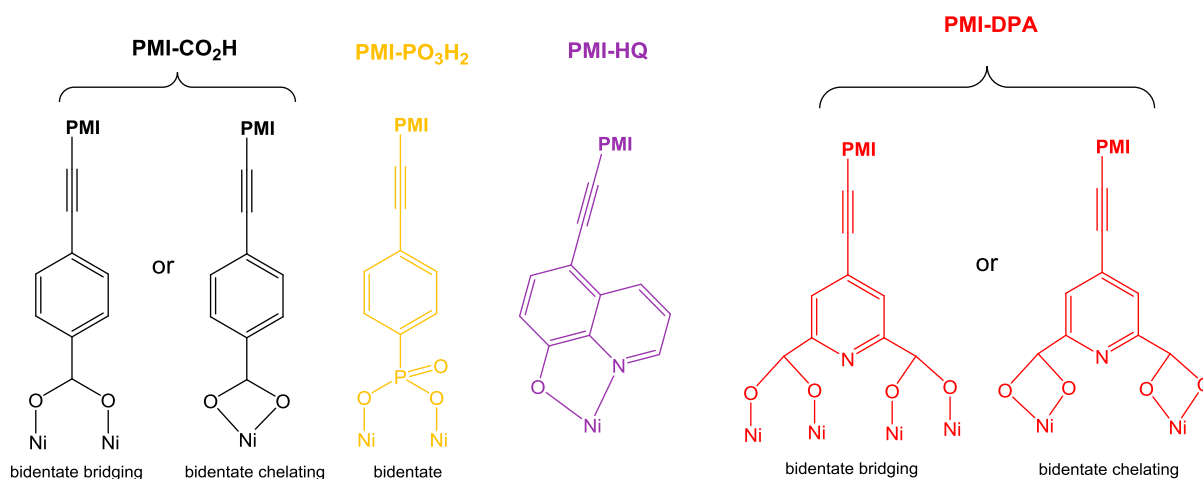


**Figure 6.** Schematic representation of the binding mode of each anchoring group.

The IR spectrum of **PMI-PO<sub>3</sub>H<sub>2</sub>** is also very rich of information owing to the numerous vibrational modes on the phosphonic acid resonator (Figure S4). After binding, the P=O stretching band at 1210 cm<sup>-1</sup> is not modified and is still intensely present, while the P-OH stretching bands between 925-940 cm<sup>-1</sup> disappears and a new band appears at 968 cm<sup>-1</sup>.<sup>[44-47]</sup> This suggests that P=O is not involved in the binding, but the two P-OH group are deprotonated and chelated to nickel, giving a bidentate binding mode as usually observed.<sup>[12]</sup> The interpretation of the IR spectrum of **PMI-HQ** can be made according to that of the Ni(II) quinolinol complex.<sup>[48-49]</sup> The  $\nu(\text{C}=\text{N})$  band of quinoline moiety, initially located at 1476 cm<sup>-1</sup> before binding, is shifted to lower wavelength number (1468 cm<sup>-1</sup>) after chelation to NiO (Figure S5). This change is typical of quinoline group coordinated to Lewis acid metals.<sup>[48-49]</sup> The observation of the  $\nu(\text{OH})$  band of the phenol is more difficult as it appears as a broad band of medium intensity around 3400 cm<sup>-1</sup> and it overlaps with those of the hydroxyl groups of NiO. However, the intensity of the  $\nu(\text{C}-\text{O})$  stretching band around 1030 cm<sup>-1</sup> has decreased after binding, in agreement with formation of a metal-oxygen bond (Figure S5). Overall, we propose that both the nitrogen and the oxygen of hydro-quinoline moiety of **PMI-HQ** are bound to Ni(II) like in coordination complex of nickel tris(hydro-quinoline) because spectra of these species share similarities (Figure 6).

The dipicolinic acid anchoring group of **PMI-DPA** raises the questions whether both carboxylic acid groups are bound to the surface and if the nitrogen of pyridyl unit participates to the binding. The first interrogation can be quickly answered as the C=O stretching band at 1730 cm<sup>-1</sup> has completely disappeared and an intense absorption at 1393 cm<sup>-1</sup> (symmetric

stretching of O-C-O) can be observed after grafting the dye on NiO (Figure S6). As a result, we can conclude that both carboxylic acid groups are involved in the binding with Ni(II). Concerning the participation of the pyridyl unit, the breathing modes of the aromatic ring due to  $\nu(\text{C}=\text{C})$  and  $\nu(\text{C}=\text{N})$  located at 1414, 1446, 1464  $\text{cm}^{-1}$  are not altered after binding, indicating that the pyridine is not coordinated to the NiO surface (Figure S6).<sup>[20, 50]</sup> This is not surprising owing to the electron withdrawing nature of the PMI unit which most certainly diminishes the electron density on the nitrogen. As a consequence, the binding mode is either bidentate chelating or bidentate bridging mode but most probably bidentate chelating for geometrical reason (Figure 6). The mode of binding of acac group in **PMI-acac** was not analyzed, because the dye loading on NiO was not sufficiently high to obtain a good quality spectrum that would enable us to make a conclusive analysis (Figure S7).

### **Stability assessment of the dye-NiO linkage**

The stability of anchoring groups in corrosive environment such as those in aqueous basic or acid conditions is an important factor to consider when designing dyes for DSPECs, because the electrode must sustain much harsher conditions than those in DSSCs. To assess the relative stabilities of each anchoring group, the stained electrodes were first soaked in acidic (acetic acid at 35 mM) or basic (tetrabutylammonium hydroxide at 1 mM) aqueous solutions, but no leaching of the dyes could be observed. This result is most certainly the consequence of the high insolubility of these hydrophobic and aromatic dyes in water as already observed with other systems.<sup>[51]</sup> Next, we turn to DMF solutions, which is a good solvent for all the dyes, to determine the relative stability scale of these series of anchoring groups. Towards this objective, the NiO electrodes, initially coated with each dye, were soaked in acidic (acetic acid at 35 mM) or in basic (tetrabutylammonium hydroxide at 1 mM) DMF solutions and the absorption of the DMF solution was monitored as a function of time for one hour (Figure 7). The dye substituted with hydroxyquinoline (PMI-HQ) anchor was not investigated with this method, because the absorption spectrum of the desorbed solution was complicated by the presence of several species (broad absorption band very different from that of the dye implying degradation) preventing thus a quantitative analysis. However for a qualitative assessment, we have tentatively ranked the relative stability of PMI-HQ by using the pictures of the NiO films before and after 5 hours of soaking (Figure S9 ESI materials).

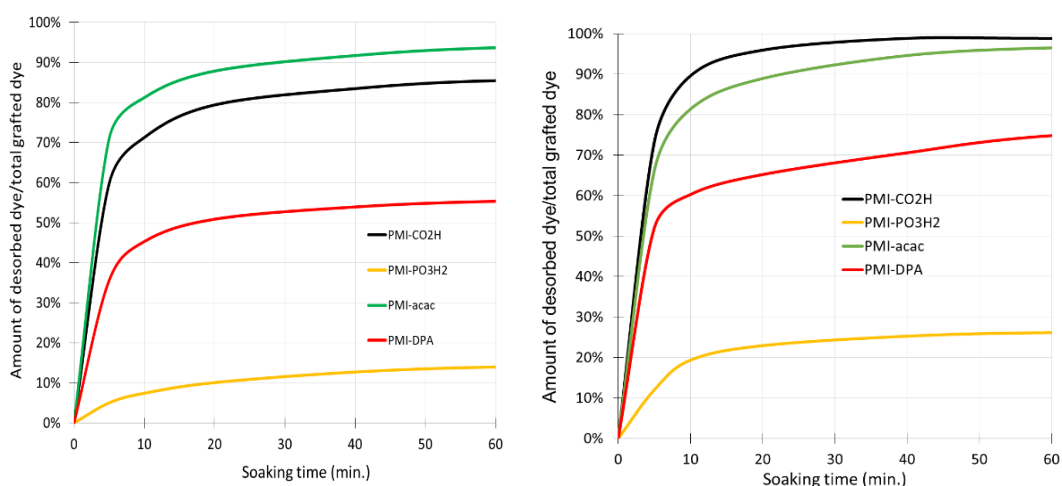


**Figure 7.** Evolution of the relative absorbance of the DMF solution as a function of soaking time of NiO electrode coated with the PMI dyes. Left panel DMF with 35 mM of acetic acid and right panel DMF with 1 mM of tetrabutylammonium hydroxide.

First, in acidic conditions the phosphonic acid anchoring group is by far the most stable linker to NiO, a result in line with the high stability already reported on TiO<sub>2</sub> surface.<sup>[52-53]</sup> On the other hand, the least stable anchoring groups are acetyl acetone and carboxylic acid (Figure 7). Interestingly, dipicolinic acid (PMI-DPA) is less desorbed than the PMI-CO<sub>2</sub>H, which contains a single carboxylic anchoring group, most probably because DPA binds with the two carboxylic groups (see IR study above). Overall, in acid conditions, the relative stability towards desorption of the anchoring groups is: PO<sub>3</sub>H<sub>2</sub> >> DPA > HQ > CO<sub>2</sub>H > acac. Please note that PMI-HQ was ranked here only according to the qualitative observation of the electrode color as a function of the soaking time (Figure S9).

As far as the basic conditions are concerned, significant differences can be noticed. First, the stability of the linkage is lower in basic conditions than in acidic ones, because all binding groups detach faster from NiO surface. This result can be understood by the fact that hydroxyl anion is a stronger competitor than water to displace the anchoring group on the PMI dye from the NiO surface. Phosphonic acid remains the most stable anchor. Single carboxylic anchoring group (PMI-CO<sub>2</sub>H) is quickly desorbed as compare to the other binding group and it is followed by acac. Overall, in basic conditions, the relative stability of the linkage is: PO<sub>3</sub>H<sub>2</sub> > DPA > HQ > acac > CO<sub>2</sub>H. Please note that PMI-HQ was ranked here only according to qualitative observation of the electrode color as a function of the soaking time (Figure S9).

In conclusion, the most stable binding group within this series is the phosphonic acid both in acidic and basic conditions. Accordingly, phosphonic acid remains among the best and most promising anchor to ensure slow desorption of a grafted molecular component on NiO surface. Dipicolinic acid does not provide as strong binding as phosphonic acid does, however, it is significantly more stable than the classically used carboxylic acid. Based on qualitative observation of the optical density of the soaked electrodes, it appears that hydroxyquinoline however provides a stronger stability than carboxylic acid.

### Quantum chemical calculations

In order to get further insights on the structural and optical properties of the dyes, the ground and lowest excited electronic states of the dyes were investigated using Density Functional Theory (DFT) and Time Dependent DFT (TD-DFT) calculations, respectively. Solvent effects were included by the means of a Polarizable Continuum Model.<sup>[54]</sup> For the sake of clarity only results computed at the LC-PBE level of theory<sup>[55]</sup> are reported in the main text while corresponding data computed at the PBE0 level<sup>[56]</sup> are reported in Supporting Information together with a more extensive description of the computational protocol. The simulated absorption spectra are reported in Figure S8. All dyes are characterized by an intense absorption band centered around 475 nm corresponding to a  $\pi-\pi^*$  excitation of dominant HOMO-LUMO character. Although the computed absorption energies are shifted by roughly 50 nm with respect to the experimental values, calculations correctly reproduce the relative shift in absorption band maxima observed for the different dyes and, in particular, the observed sizable red-shifted absorption of **PMI-HQ** and **PMI-NH<sub>2</sub>** (Figure 8). Indeed, calculations show that due to the electron donating effect of the aniline and hydroxyquinoline groups, for these two dyes the HOMO lies at higher energy resulting in a consequently reduced HOMO-LUMO gap as reported in Figure 9. In particular, while the LUMO (of  $\pi^*$  character) is practically unchanged for all systems and always localized on the PMI moiety, the HOMO (of  $\pi$  character) shows a partial delocalization on the anchoring moiety only in the case of the **PMI-NH<sub>2</sub>** and **PMI-HQ** molecules and, to a minor extent, also in the case of the PMI-acac system. Therefore, the first electronic transition computed for all these systems of dominant HOMO-LUMO character displays a sizable intramolecular Charge Transfer (ICT) nature. This ICT character has been quantified computing the associated effective hole electron distance by the means of the  $D_{CT}$  index.<sup>[57-58]</sup> Accordingly, **PMI-HQ** and **PMI-NH<sub>2</sub>** molecules display the greatest  $D_{CT}$  value among the six molecules tested (Table 3), thus in



principle providing the best hole-electron separation upon excitation followed by PMI-acac. On the other hand, the smallest ICT character is computed for the **PMI-DPA** system.

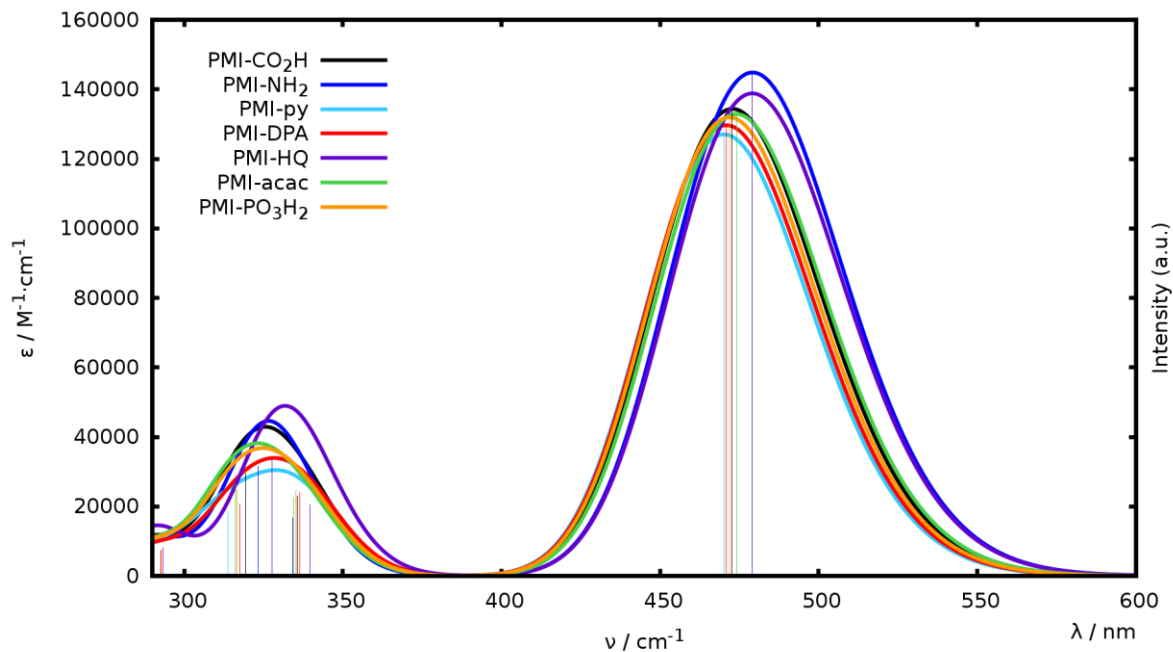


**Figure 8.** Simulated electronic absorption spectra of the dyes.

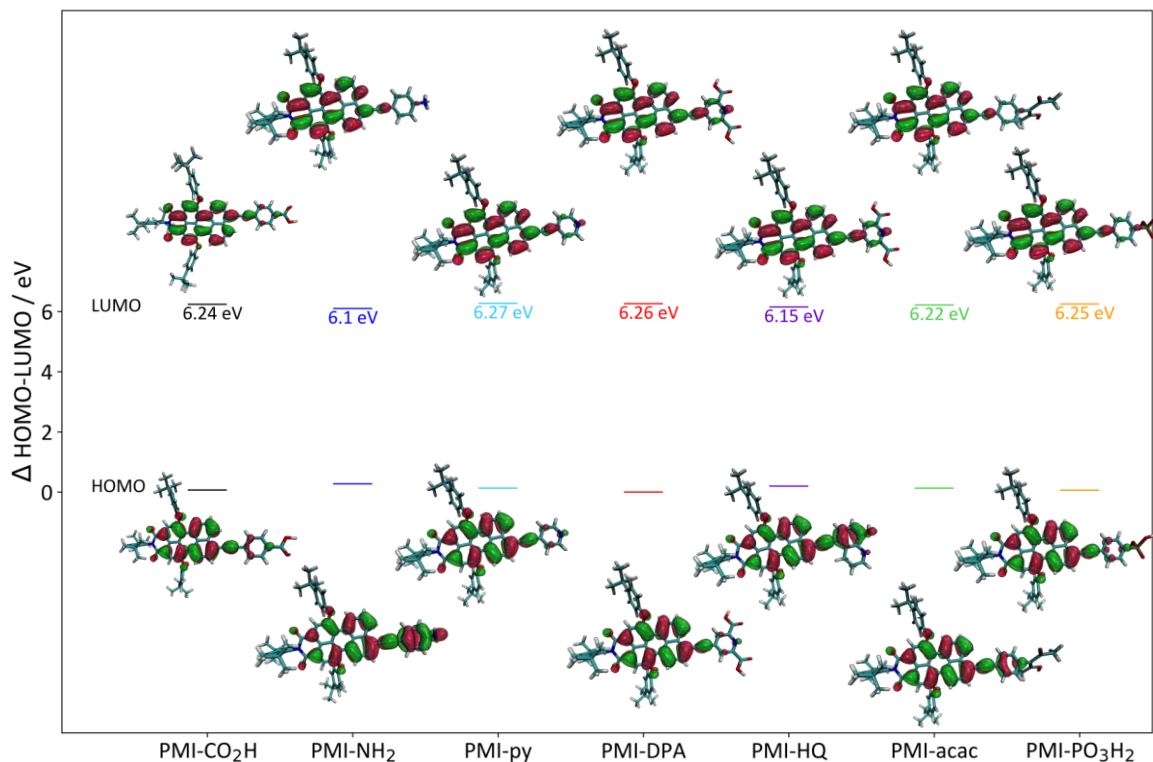


**Figure 9.** HOMO-LUMO energies and gaps (in eV), where the former are given relative to the HOMO energy of **PMI-DPA**.

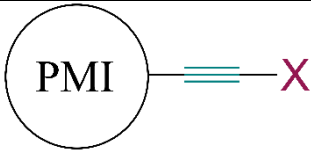
**Table 3.** Computed absorption energies ( $\lambda_{\text{abs}}$  in nm) and associated oscillator strengths (in au) and  $D_{\text{CT}}$  values (in Å).

Dye	$\lambda_{\text{abs}}$	Oscillator Strength	$D_{\text{CT}}/\text{Å}$
<b>PMI-CO<sub>2</sub>H</b>	473	1.71	1.83
<b>PMI-NH<sub>2</sub></b>	479	1.85	2.64
<b>PMI-py</b>	470	1.62	1.81
<b>PMI-HQ</b>	479	1.77	2.33
<b>PMI-DPA</b>	471	1.65	1.54
<b>PMI-acac</b>	474	1.70	2.21
<b>PMI-PO<sub>3</sub>H<sub>3</sub></b>	472	1.68	1.90

Calculation of the reduced form of the dyes allowed quantification of the spin density localized on each of the moieties that are here defined as the PMI core and the anchoring groups (-C≡C-X). The contribution of the anchoring group has been further dissected in the one localized on the carbon-carbon triple bond and on the terminal group (X) as reported in Table 4. In agreement with the LUMO localization on the PMI core, the spin density is

mainly localized on it. Furthermore, the spin density distributes similarly among the terminal groups (-X) and carbon-carbon triple bonds. The terminal groups indeed carry from 3 to 4 % of the total spin density while the carbon-carbon triple bond carries from 2 to 4 % of the total spin density. The highest spin density contribution on the anchoring group is computed for the PMI-DPA (7.5%) while only in the case of PMI-NH<sub>2</sub> and PMI-CO<sub>2</sub>H an excess of beta spin density (resulting from a spin polarization effect) is computed. Nonetheless, these variations are relatively small and, in a general sense, we can conclude that the spin delocalization on the dyes is relatively insensitive to the anchoring group considered.

**Table 4.** Computed Mulliken spin densities of the dyes, localized on the anchoring  $\text{-C}\equiv\text{C-X}$  group, along with the repartition on the carbon-carbon triple bond -  $\text{C}\equiv\text{C}$  and on the terminal group  $\text{-X}$ .



	PMI-CO <sub>2</sub> H	PMI-NH <sub>2</sub>	PMI-py	PMI-DPA	PMI-HQ	PMI-Acac	PMI-PO <sub>3</sub> H <sub>2</sub>
$\text{-C}\equiv\text{C-X}$	-0.197	-0.022	0.065	0.075	0.065	0.057	0.064
$\text{-X}$	-0.026	-0.043	0.037	0.036	0.034	0.036	0.039
$\text{-C}\equiv\text{C}$	-0.171	0.021	0.029	0.039	0.031	0.022	0.024
PMI	1.197	1.022	0.935	0.925	0.935	0.945	0.936

### Transient absorption spectroscopy of the PMI dyes

The different anchor groups may lead to significant variations in electronic coupling to the NiO within the series of dyes. To investigate potential resulting differences in hole injection and recombination, transient absorption (TA) was performed on the dyes in solution and

grafted on NiO. When exciting **PMI-CO<sub>2</sub>H** in THF solution, the transient absorption spectra show negative features from 480 nm to 650 nm and positive induced absorption features in the rest of the spectral range (Figure 10, left).

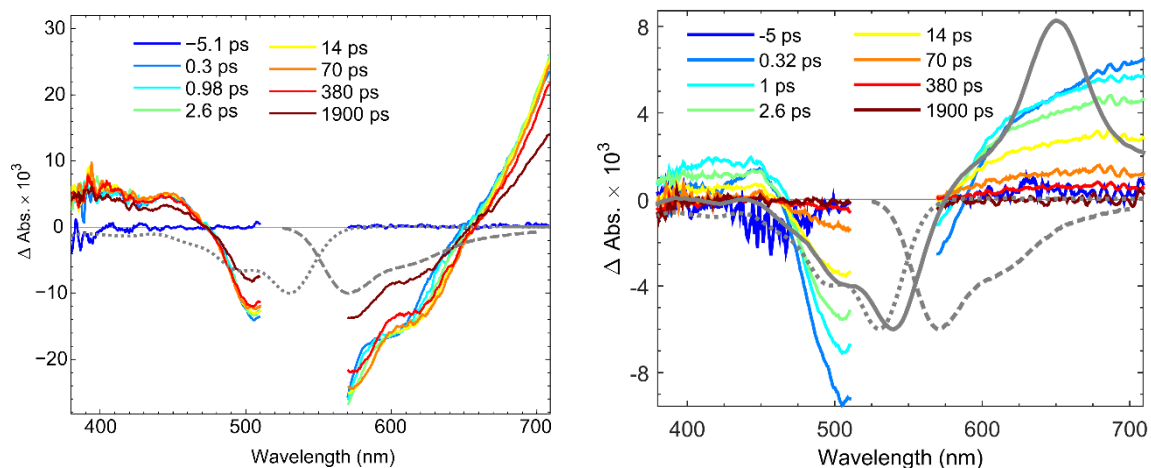


**Figure 10.** Transient absorption spectra of **PMI-CO<sub>2</sub>H** in THF solution (left) and grafted on NiO films, immersed in propylene carbonate solution (right) at different time delays after excitation at 540 nm. The gray lines represent the corresponding ground state absorption (dotted) and fluorescence (dashed) spectra and the difference spectrum from spectroelectrochemical reduction (full) in arbitrary units.

The shape of the bleach resembles a superposition of the negative ground state absorption and fluorescence, hence being a sum of ground state bleach and stimulated emission. Therefore, this spectrum can be assigned to the singlet excited state of **PMI-CO<sub>2</sub>H**. The other PMIs that show very similar ground state absorption and fluorescence spectra, namely **PMI-acac**, **PMI-PO<sub>3</sub>H<sub>2</sub>**, **PMI-DPA** and **PMI-Py**, are expected to exhibit similar transient absorption spectra. The TA of **PMI-HQ**, which has a broader absorption spectrum, was investigated as well. It shows similar features as **PMI-CO<sub>2</sub>H** except for a Stokes-shift of the stimulated emission with a biphasic behavior with time constants of 2 ps and 7.6 ps (Figure S11).

When grafting **PMI-CO<sub>2</sub>H** on mesoporous NiO, the TA spectra change (Figure 10, right). The ground state bleach is narrower (from 460 nm to 580 nm). There is no stimulated emission indicating that the singlet excited state has decayed within the experimental time resolution. The shape of the TA spectrum resembles the reduced state of **PMI-CO<sub>2</sub>H** indicating ultrafast (<200 fs) hole injection, as commonly found for NiO-based DSSCs.<sup>[2, 11]</sup>

<sup>59]</sup> However, the spectral shape does not completely follow the reference of the reduced state. This could be explained by a broadening of the peak at 650 nm due to different environment. A similar broadening was observed earlier.<sup>24</sup> It could, however, also originate from dye aggregates on the surface, for which the anion spectra are different than for the monomers. The other dyes show very similar TA spectra (not shown) and kinetic traces (Figure 11). However, **PMI-HQ** shows a contribution from stimulated emission in the initial spectra ( $< 1$  ps) suggesting a slower injection for this compound (Figure S14 and Figure S15).

When comparing the normalized kinetics of the PMIs grafted on NiO in propylene carbonate solution, there is no significant difference between those of **PMI-CO<sub>2</sub>H**, **PMI-acac**, **PMI-DPA**, **PMI-PO<sub>3</sub>H<sub>2</sub>**, and **PMI-HQ** shows a fast component in the ground state bleach recovery, which is attributed to the disappearance of the stimulated emission, i.e. reflecting hole injection. This processes is, however, still on the sub-ps time scale. Except for this difference, the TA signal of the reduced PMIs decays non-exponentially to approximately 20% of the initial signal after 1.9 ns.

When adding the T<sub>2</sub>/T<sup>-</sup> electrolyte, the kinetics is slightly slower compared to the kinetics in propylene carbonate only. Also with T<sub>2</sub>/T<sup>-</sup>, the signal decays to approximately 20% of the initial value at 1.9 ns. There are previous studies where the dye anion has been more long-lived in the presence of redox couple than without.<sup>[60]</sup> This counter-intuitive result must be attributed to changes in the fermi level (hole filling by the electrolyte), which slows down dye-NiO recombination. This makes it difficult to estimate the regeneration efficiency, and may obscure differences in recombination and regeneration rates between dyes. Especially for **PMI-acac**, the fraction of the initial signal that remains (20%) is smaller lower than the IPCE value (30 %, see below), indicating that (some) regeneration should take place on the sub-ns timescale.

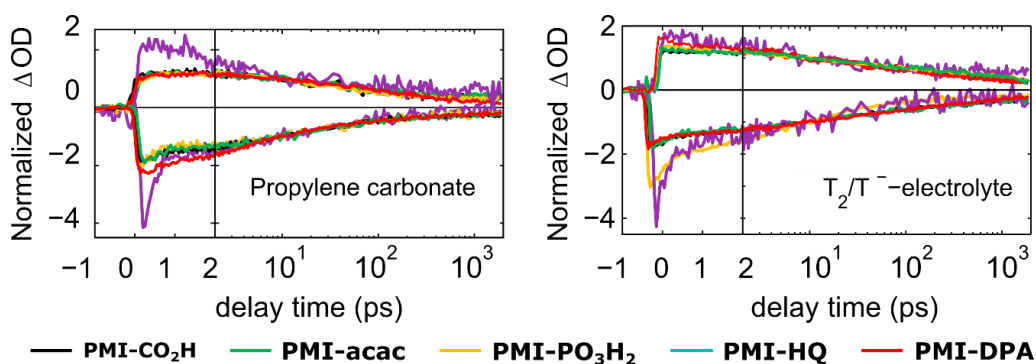


**Figure 11.** Kinetic traces of the TA at the maximum of the induced absorption and the minimum of the ground state bleach of PMI sensitized NiO films in propylene carbonate (upper/left) and the E3 electrolyte  $T_2/T^-$  (bottom/right) after excitation at 540 nm and normalized at 10 ps.

To summarize, all investigated PMIs inject on a sub-ps time scale and show very similar recombination kinetics. Hence, the anchoring group does not seem to significantly influence the photophysical or electron transfer properties. Given the very different electronic structures of the anchoring groups, this is a surprising result. One possible reason is that hole injection and charge recombination does not occur through-bond but predominantly through space, as the dyes may lie close to the NiO surface.<sup>[61-63]</sup> Another possibility is that the hole injection is very fast and may be best described as adiabatic. In this case, the rate is not sensitive to small variations of the electronic coupling of the dye with the semiconductor. This is why there is no noticeable difference in the injection rate constants from one anchoring group to the others.

There are no obvious effects on the dynamics that can be attributed to dye aggregates (Figure 10). To study whether the aggregation has an effect on the conversion efficiency, PV measurements of DSSCs were conducted. The results are presented below.

### **Photovoltaic performances of the PMI dyes in p-DSSCs**

The PMI dyes were used to fabricate p-DSSC with a NiO sensitized film assembled to a platinized counter electrode (See experimental part for fabrication details). A preliminary study was conducted only with **PMI-CO<sub>2</sub>H** dye with three electrolyte compositions in order to identify the optimized electrolyte for these sensitizers. Electrolytes with two different compositions of iodine/triiodide as redox couple and another one with 1-methyl-1H-tetrazole-5-thiolate (T-) and its disulfide dimer (T<sub>2</sub>)<sup>[35]</sup> were investigated (Table 5).

**Table 5.** Photovoltaic properties of the p-DSSCs recorded under simulated AM 1.5 with **PMI-CO<sub>2</sub>H** sensitizer.

Electrolyte	$J_{sc}$ [mA.cm <sup>-2</sup> ]	$V_{oc}$ [mV]	FF [%]	$\eta$ [%]
$I_3^-/I^-$ (E1)	$1.50 \pm 0.15$	$72 \pm 4$	$30.4 \pm 0.3$	$0.032 \pm 0.005$
$I_3^-/I^-$ (E2)	$0.36 \pm 0.01$	$106 \pm 2$	$25.7 \pm 0.4$	$0.010 \pm 0.000$
$T_2/T^-$ (E3)	$1.46 \pm 0.05$	$160 \pm 3$	$24.2 \pm 0.2$	$0.056 \pm 0.002$

E1 composition:  $[I_2] = 0.1$  M,  $[LiI] = 1$  M in  $CH_3CN$ ; E2 composition:  $[I_2] = 0.03$  M,  $[1,2\text{-dimethyl-3-butylimidazolium iodide}] = 0.6$  M,  $[tBu\text{-pyridine}] = 0.5$  M,  $[guanidinium thiocyanate] = 0.1$  M, in  $CH_3CN$ ; E3 composition:  $[T_2] = 0.3$  M,  $[T^-] = 0.1$  M,  $[LiTFSI] = 0.1$  M in propylene carbonate/ $CH_3CN$ : 3/7 vol./vol.)

With the iodine based electrolyte, the one richer in triiodide (E1) gave the highest photocurrent density, while the redox couple  $T_2/T^-$  performs similarly in terms of  $J_{sc}$  but gives a higher  $V_{oc}$ . Moreover and very importantly, the latter redox couple does not produce photocurrents from light absorption by the electrolyte, as observed for iodine based electrolytes, especially when they contain a high concentration of triiodide.<sup>[64-65]</sup> This is clearly visible in the photoaction spectra, which features a prominent band between 350-420 nm attributed to the photoactivity of triiodide (Figure S16). Therefore, the rest of the photovoltaic study was conducted with electrolyte E3 composed of the  $T_2/T^-$  redox mediator because it gives the highest performance and is not unreliably biased with artefacts on the photocurrent densities. The metrics of the solar cells of all the other PMI dyes fabricated with the  $T_2/T^-$  electrolyte are gathered in Table 6 and the IPCE spectra are given in Figure 12.

**Table 6.** Photovoltaic properties of the p-DSSCs recorded under simulated AM 1.5 with all the PMI sensitizers with the electrolyte E3 composed of the  $T_2/T^-$  redox mediator.

Dyes	$J_{sc}$ [mA.cm <sup>-2</sup> ]	$V_{oc}$ [mV]	FF [%]	$\eta$ [%]	Dye loading [nmol cm <sup>-2</sup> ]
<b>PMI-CO<sub>2</sub>H</b>	$1.52 \pm 0.06$	$161 \pm 7$	$25.4 \pm 0.3$	$0.062 \pm 0.001$	22.3
<b>PMI-HQ</b>	$2.21 \pm 0.09$	$164 \pm 4$	$23.8 \pm 0.6$	$0.086 \pm 0.003$	9.3
<b>PMI-DPA</b>	$1.33 \pm 0.09$	$168 \pm 6$	$24.6 \pm 0.6$	$0.055 \pm 0.005$	23.7
<b>PMI-acac</b>	$2.08 \pm 0.08$	$169 \pm 8$	$27.9 \pm 0.2$	$0.098 \pm 0.002$	7.7
<b>PMI-PO<sub>3</sub>H<sub>2</sub></b>	$1.27 \pm 0.12$	$181 \pm 7$	$17.7 \pm 0.4$	$0.041 \pm 0.004$	38.2

Interestingly, the photovoltaic performances of these dyes differ significantly from one to another with **PMI-HQ** and **PMI-acac** being the most efficient within these series. There is a strong correlation between the dye loading and the short circuit photocurrent density, with the unusual behavior that  $J_{SC}$  decreases with increasing dye loading. This is most certainly the direct consequence of the formation of aggregates on NiO, which decreases the injection quantum yield owing to quenching of the excited state. Consequently, the difference in photovoltaic performances of these dyes is not predominantly controlled by the anchoring groups in a direct way, but by the degree of aggregate formation. The latter increases with increasing dye loading that is, however, controlled by the affinity of the anchoring group with the NiO surface. Nevertheless, the IPCE spectra still show larger values at the higher vibronic peak (ca. 500 nm) than at the lower one (ca. 550 nm). Thus, it is clear that the aggregated dyes do contribute to the photocurrent, albeit with a lower yield than for the monomeric dyes. However, we have tested the possibility to break the aggregates by loading the **PMI-PO<sub>3</sub>H<sub>2</sub>** dye in presence of increasing concentrations of chenodeoxycholic acid (CDCA) ([CDCA] = 2 mM, 5 mM, 10 mM and 20 mM) into the dyeing bath, hence a dye/CDCA ratios of 0, 10, 25, 50 and 100 were explored. However, the  $J_{sc}$  and the  $V_{oc}$  was not changed within experimental errors resulting in no real improvement of the PCE. In a second series of experiments, we have also investigated the possibility to reduce the degree of dye aggregation by shortening the soaking time. The NiO electrodes were therefore soaked into the dye bath for 30 minutes, 2 hours, 4 hours and overnight. It turned out that after 2 hours, the  $J_{sc}$  and  $V_{oc}$  plateau to almost the same values measured after 12 hours. When the soaking time was set to 30 min, both  $J_{sc}$  and  $V_{oc}$  were reduced by about 20% relative to those after overnight in line with the lower dye concentration on the NiO film. Overall, we conclude that the control of the dye aggregation on NiO surface with **PMI-PO<sub>3</sub>H<sub>2</sub>** cannot be simply achieved neither with CDCA used as co-adsorbent in the dyeing bath nor by reducing the soaking time. Probably, the aggregates already form in the dyeing bath before chemisorption.



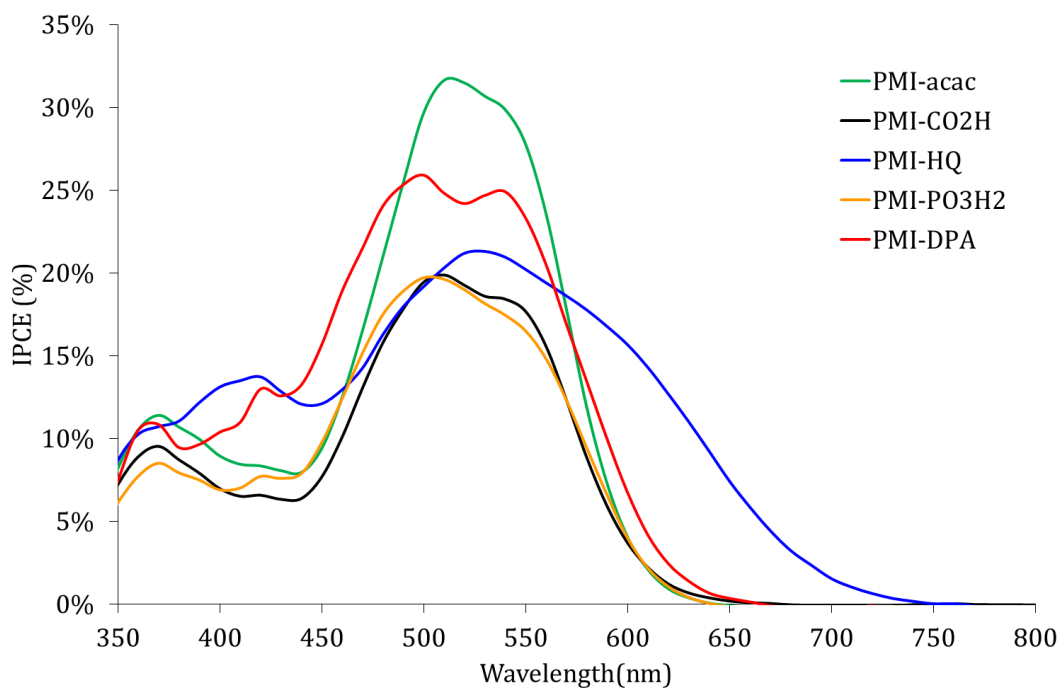


**Figure 12.** IPCE spectra of the PMI dyes recorded with the electrolyte composed of the  $T_2/T^+$  redox mediator.

## Conclusion

In this study, we have investigated the largest series of anchoring groups for dyes sensitizing NiO. A series of seven different anchoring groups was explored with regard to their ability to form strong linkage with NiO and to mediate electronic coupling with the NiO valence band. Overall, we found that phosphonic acid is the strongest binding group of the series and it leads to the highest dye loading. Conversely, acac and hydroxyquinoline are the weakest binding groups. Moreover, dipicolinic acid proved to be a stronger anchor than carboxylic. The photophysical study reveals that the PMI excited state of all dyes is quenched by fast hole injection into NiO at a sub-ps time scale, irrespectively of the binding group. Similarly, the anchoring group had no effect on the charge recombination kinetics. The weakest binding groups led to the lowest dye loading and consequently to the lowest degree of aggregation on NiO, which results in the highest photovoltaic performances, even if the differences are small. This demonstrates that, for dyes which have a strong tendency to form aggregates, the strongest binding group is not necessary optimal for application in DSSCs. This study also shows that the investigated anchor groups work equally well for hole injection and dye regeneration and therefore that the anchor-mediated electronic coupling of the dye with the semiconductor in NiO based DSSC may not be the primary parameter to consider to slow

down the charge recombination between the reduced dye and the holes in NiO valence band. However, for the fabrication of DSPEC, phosphonic acid is the most favorable binding group, within those investigated in these series, to attach a dye or a catalyst to NiO surface.

### Acknowledgments

The authors are grateful to Agence Nationale de la Recherche (ANR) for the financial support of these researches through the program POSITIF (ANR-12-PRGE-0016-01) and Région des Pays de la Loire for the project LUMOMAT, to the Swedish Research Council (Project no 2014-5921) and the Swedish Energy Agency (Project no 4359-1). IC and FM have received funding from the European Research Council (ERC) under the European Union's Horizon 2020 research and innovation program (grant agreement No 648558).

### References

- [1] A. Nattestad, A. J. Mozer, M. K. R. Fischer, Y. B. Cheng, A. Mishra, P. Baeuerle, U. Bach, *Nat. Mater.* **2010**, *9*, 31-35.
- [2] E. A. Gibson, A. L. Smeigh, L. L. Pleux, J. Fortage, G. Boschloo, E. Blart, Y. Pellegrin, F. Odobel, A. Hagfeldt, L. Hammarström, *Angew. Chem. Int. Ed.* **2009**, *48*, 4402-4405.
- [3] Y. Farré, M. Raissi, A. Fihey, Y. Pellegrin, E. Blart, D. Jacquemin, F. Odobel, *ChemSusChem* **2017**, *10*, 2618-2625.
- [4] F. Li, K. Fan, B. Xu, E. Gabrielsson, Q. Daniel, L. Li, L. Sun, *J. Am. Chem. Soc.* **2015**, *137*, 9153-9159.
- [5] K. A. Click, D. R. Beauchamp, Z. Huang, W. Chen, Y. Wu, *J. Am. Chem. Soc.* **2016**, *138*, 1174-1179.
- [6] L. Tong, A. Iwase, A. Nattestad, U. Bach, M. Weidelener, G. Gotz, A. Mishra, P. Bäuerle, R. Amal, G. G. Wallace, A. J. Mozer, *Energy Environ. Sci.* **2012**, *5*, 9472-9475.
- [7] E. A. Gibson, *Chem. Soc. Rev.* **2017**, *46*, 6194-6209.
- [8] D. L. Ashford, M. K. Gish, A. K. Vannucci, M. K. Brennaman, J. L. Templeton, J. M. Papanikolas, T. J. Meyer, *Chem. Rev.* **2015**, *115*, 13006-13049.
- [9] V. Nikolaou, A. Charisiadis, G. Charalambidis, A. G. Coutsolelos, F. Odobel, *J. Mater. Chem. A* **2017**, *5*, 21077-21113.
- [10] F. Odobel, Y. Pellegrin, *Journal of Physical Chemistry Letters* **2013**, *4*, 2551-2564.

- [11] F. Odobel, Y. Pellegrin, E. A. Gibson, A. Hagfeldt, A. L. Smeigh, L. Hammarström, *Coord. Chem. Rev.* **2012**, *256*, 2414-2423.
- [12] K. L. Materna, R. H. Crabtree, G. W. Brudvig, *Chem. Soc. Rev.* **2017**, *46*, 6099-6110.
- [13] L. Zhang, J. M. Cole, *ACS Appl. Mater. Interfaces* **2015**, *7*, 3427-3455.
- [14] B. O'Regan, M. Grätzel, *Nature* **1991**, *353*, 737.
- [15] A. Hagfeldt, G. Boschloo, L. Sun, L. Kloo, H. Pettersson, *Chem. Rev.* **2010**, *110*, 6595-6663.
- [16] R. Jose, A. Kumar, V. Thavasi, K. Fujihara, S. Uchida, S. Ramakrishna, *Appl. Phys. Lett.* **2008**, *93*, 023125.
- [17] Y. Pellegrin, L. Le Pleux, E. Blart, A. Renaud, B. Chavillon, N. Szuwarski, M. Boujtita, L. Cario, S. Jobic, D. Jacquemin, F. Odobel, *J. Photochem. Photobiol., A* **2011**, *219*, 235-242.
- [18] J. Warnan, Y. Pellegrin, E. Blart, L. Zhang, A. Brown, L. Hammarström, D. Jacquemin, F. Odobel, *Dyes and Pigments* **2014**, *105*, 174-179.
- [19] M. Wykes, F. Odobel, C. Adamo, I. Ciofini, F. Labat, *J. Mol. Model.* **2016**, *22*, 289.
- [20] J. Cui, J. Lu, X. Xu, K. Cao, Z. Wang, G. Alemu, H. Yuang, Y. Shen, J. Xu, Y. Cheng, M. Wang, *J. Phys. Chem. C* **2014**, *118*, 16433-16440.
- [21] B. Jin, W. J. Wu, X. Y. Zhang, F. L. Guo, Q. Zhang, J. L. Hua, *Chem. Lett.* **2013**, *42*, 1271-1272.
- [22] Y. Yu, X. Li, Z. Shen, X. Zhang, P. Liu, Y. Gao, T. Jiang, J. Hua, *J. Colloid Interface Sci.* **2017**, *490*, 380-390.
- [23] F. A. Black, C. J. Wood, S. Ngwerume, G. H. Summers, I. P. Clark, M. Towrie, J. E. Camp, E. A. Gibson, *Faraday Discussions* **2017**, *198*, 449-461.
- [24] G. H. Summers, G. Lowe, J.-F. Lefebvre, S. Ngwerume, M. Bräutigam, B. Dietzek, J. E. Camp, E. A. Gibson, *ChemPhysChem* **2017**, *18*, 406-414.
- [25] K. Yun, S. Zhang, F. Yu, H. Ye, J. Hua, *J. Energy Chem.* **2018**, *27*, 728-735.
- [26] A. Sinopoli, F. A. Black, C. J. Wood, E. A. Gibson, P. I. P. Elliott, *Dalton Trans.* **2017**, *46*, 1520-1530.
- [27] D. Gosztola, M. P. Niemczyk, W. Svec, A. S. Lukas, M. R. Wasielewski, *J. Phys. Chem. A* **2000**, *104*, 6545-6551.
- [28] A. Morandeira, J. Fortage, T. Edvinsson, L. Le Pleux, E. Blart, G. Boschloo, A. Hagfeldt, L. Hammarström, F. Odobel, *J. Phys. Chem. C* **2008**, *112*, 1721-1728.

- [29] J. M. Giaimo, A. V. Gusev, M. R. Wasielewski, *J. Am. Chem. Soc.* **2002**, *124*, 8530-8531.
- [30] T. van der Boom, R. T. Hayes, Y. Zhao, P. J. Bushard, E. A. Weiss, M. R. Wasielewski, *J. Am. Chem. Soc.* **2002**, *124*, 9582-9590.
- [31] Z. Chen, B. Fimmel, F. Wurthner, *Org. Biomol. Chem.* **2012**, *10*, 5845-5855.
- [32] D. Ameline, S. Diring, Y. Farre, Y. Pellegrin, G. Naponiello, E. Blart, B. Charrier, D. Dini, D. Jacquemin, F. Odobel, *RSC Adv.* **2015**, *5*, 85530-85539.
- [33] J. He, H. Lindström, A. Hagfeldt, S.-E. Lindquist, *J. Phys. Chem. B* **1999**, *103*, 8940-8943.
- [34] G. Boschloo, A. Hagfeldt, *Acc. Chem. Res.* **2009**, *42*, 1819-1826.
- [35] X. Xu, B. Zhang, J. Cui, D. Xiong, Y. Shen, W. Chen, L. Sun, Y. Cheng, M. Wang, *Nanoscale* **2013**, *5*, 7963-7969.
- [36] Y. Hao, C. J. Wood, C. A. Clark, J. A. Calladine, R. Horvath, M. W. D. Hanson-Heine, X.-Z. Sun, I. P. Clark, M. Towrie, M. W. George, X. Yang, L. Sun, E. A. Gibson, *Dalton Trans.* **2016**, *45*, 7708-7719.
- [37] M. Brautigam, J. Kubel, M. Schulz, J. G. Vos, B. Dietzek, *Phys. Chem. Chem. Phys.* **2015**, *17*, 7823-7830.
- [38] F. Porta, S. Recchia, C. Bianchi, F. Confalonieri, G. Scari, *Colloids and Surfaces A: Physicochemical and Engineering Aspects* **1999**, *155*, 395-404.
- [39] L. Durand-Keklikian, I. Haq, E. Matijević, *Colloids and Surfaces A: Physicochemical and Engineering Aspects* **1994**, *92*, 267-275.
- [40] K. S. Finnie, J. R. Bartlett, J. L. Woolfrey, *Langmuir* **1998**, *14*, 2744-2749.
- [41] M. Nara, H. Torii, M. Tasumi, *J. Phys. Chem.* **1996**, *100*, 19812-19817.
- [42] M. Yanagida, T. Yamaguchi, M. Kurashige, K. Hara, R. Katoh, H. Sugihara, H. Arakawa, *Inorg. Chem.* **2003**, *42*, 7921-7931.
- [43] C. Bauer, G. Boschloo, E. Mukhtar, A. Hagfeldt, *J. Chem. Phys. B* **2002**, *106*, 12693-12704.
- [44] T. Undabeytia, E. Morillo, C. Maqueda, *J. Agric. Food Chem.* **2002**, *50*, 1918-1921.
- [45] W. Gao, L. Dickinson, C. Grozinger, F. G. Morin, L. Reven, *Langmuir* **1996**, *12*, 6429-6435.
- [46] G. Guerrero, P. H. Mutin, A. Vioux, *Chem. Mater.* **2001**, *13*, 4367-4373.
- [47] R. Quiñones, A. Raman, E. S. Gawalt, *Thin Solid Films* **2008**, *516*, 8774-8781.

- [48] I. Potočňák, P. Vranec, V. Farkasová, D. Sabolová, M. Vataščinová, J. Kudláčová, I. D. Radojević, L. R. Čomić, B. S. Markovic, V. Volarevic, N. Arsenijevic, S. R. Trifunović, *J. Inorg. Biochem.* **2016**, *154*, 67-77.
- [49] K. Siddappa, N. S. Mayana, *Bioinorg. Chem. Applications* **2014**, *2014*, 11.
- [50] Y. Harima, T. Fujita, Y. Kano, I. Imae, K. Komaguchi, Y. Ooyama, J. Ohshita, *J. Phys. Chem. C* **2013**, *117*, 16364-16370.
- [51] L. A. Martini, G. F. Moore, R. L. Milot, L. Z. Cai, S. W. Sheehan, C. A. Schmuttenmaer, G. W. Brudvig, R. H. Crabtree, *J. Phys. Chem. C* **2013**, *117*, 14526-14533.
- [52] K. J. Young, L. A. Martini, R. L. Milot, R. C. Snoeberger, V. S. Batista, C. A. Schmuttenmaer, R. H. Crabtree, G. W. Brudvig, *Coord. Chem. Rev.* **2012**, *256*, 2503-2520.
- [53] S. A. Paniagua, A. J. Giordano, O. N. L. Smith, S. Barlow, H. Li, N. R. Armstrong, J. E. Pemberton, J.-L. Brédas, D. Ginger, S. R. Marder, *Chem. Rev.* **2016**, *116*, 7117-7158.
- [54] V. Barone, M. Cossi, *J. Phys. Chem. A* **1998**, *102*, 1995-2001.
- [55] H. Iikura, T. Tsuneda, T. Yanai, K. Hirao, *J. Chem. Phys.* **2001**, *115*, 3540-3544.
- [56] C. Adamo, V. Barone, *J. Chem. Phys.* **1999**, *110*, 6158-6170.
- [57] T. Le Bahers, C. Adamo, I. Ciofini, *J. Chem. Theory Comput.* **2011**, *7*, 2498-2506.
- [58] F. Maschietto, M. Campetella, J. Frisch Michael, G. Scalmani, C. Adamo, I. Ciofini, *J. Comput. Chem.* **2018**, *39*, 735-742.
- [59] M. Gennari, F. Légalité, L. Zhang, Y. Pellegrin, E. Blart, J. Fortage, A. M. Brown, A. Deronzier, M.-N. Collomb, M. Boujtita, D. Jacquemin, L. Hammarström, F. Odobel, *J. Phys. Chem. Lett.* **2014**, *5*, 2254-2258.
- [60] F. A. Black, C. A. Clark, G. H. Summers, I. P. Clark, M. Towrie, T. Penfold, M. W. George, E. A. Gibson, *Phys. Chem. Chem. Phys.* **2017**, *19*, 7877-7885.
- [61] C.-W. Chang, L. Luo, C.-K. Chou, C.-F. Lo, C.-Y. Lin, C.-S. Hung, Y.-P. Lee, E. W.-G. Diau, *J. Phys. Chem. C* **2009**, *113*, 11524-11531.
- [62] P. G. Johansson, Y. Zhang, G. J. Meyer, E. Galoppini, *Inorg. Chem.* **2013**, *52*, 7947-7957.
- [63] S. Ye, A. Kathiravan, H. Hayashi, Y. Tong, Y. Infahsaeng, P. Chabera, T. Pascher, A. P. Yartsev, S. Isoda, H. Imahori, V. Sundström, *J. Phys. Chem. C* **2013**, *117*, 6066-6080.
- [64] H. Zhu, A. Hagfeldt, G. Boschloo, *J. Phys. Chem. C* **2007**, *111*, 17455-17458.
- [65] E. A. Gibson, L. Le-Pleux, J. Fortage, Y. Pellegrin, E. Blart, F. Odobel, A. Hagfeldt, G. Boschloo, *Langmuir* **2012**, *28*, 6485-6493.



## Graphical abstract for entry

